

**GT2023-102635**

## COMPARISON OF DIRT DEPOSITION ON DOUBLE-WALLED COMBUSTOR LINER GEOMETRIES

**Brandon Fallon, Kyle McFerran, Sarah Fox,  
Karen A. Thole, and Stephen P. Lynch**  
The Pennsylvania State University  
Department of Mechanical Engineering  
University Park, PA 16802, USA

**Ryan Lundgreen and  
Stephen Kramer**  
Pratt & Whitney  
East Hartford, CT 06118, USA

### ABSTRACT

Gas turbine engines are frequently subjected to particle laden flows in which dirt and sand are ingested into the hot section. The particles enter internal cooling channels where they deposit and block cooling features, creating increased heat transfer, reduced flows, and diminished cooling performance. This study investigates geometries with the intention of mitigating dirt effects on cooling for double-walled combustor liners that use impingement and effusion cooling. Dirt particulate was injected into several double-walled coupons at room temperature using two feed modes: slug and continuous. Slug feed tests used controlled bursts of dirt whereas continuous feed provided a steady stream of dirt. Computational studies were also conducted to investigate internal flow fields between the impingement and effusion plates. The best performing geometry that was tested in terms of the lowest measured dirt capture had pins and cones extruded from the cold-side of the effusion plate. The flow parameter was found to scale the dirt capture with higher capture efficiency at higher flow parameters.

### NOMENCLATURE

$A_f$	impingement flow area
$D_e$	effusion hole diameter
$D_i$	impingement hole diameter
$D_{int}$	total mass of dirt that reached the coupon
$d$	particle diameter
$FP$	flow parameter
$FP_{clean}$	flow parameter before dirt injection
$FP_{dirty}$	flow parameter after dirt injection
$H$	distance from effusion to impingement plate
$k$	ratio of specific heats
$M_{cl}$	mass of effusion plate before dirt testing
$M_{eff}$	mass of effusion plate after dirt testing
$Ma$	Mach number, $U_{jet} \cdot (k \cdot R_u \cdot T_{0C})^{-1/2}$
$\dot{m}$	mass flow rate
$N$	number of impingement holes
$P_{0C}$	supply fluid pressure

$P_\infty$	exit static pressure
PCA	pin-cone aligned
PCS	pin-cone staggered
PR	pressure ratio
$R$	individual gas constant
$R_u$	ideal gas constant
$Re_d$	jet Reynolds number, $\rho \cdot U_{jet} \cdot D_i \cdot \mu^{-1}$
RFP	Reduced flow parameter
$S_1$	pitch spacing between impingement holes
$S_2$	pitch spacing between impingement holes
$St$	Stokes number, $\rho_d \cdot d^2 \cdot U_{jet} \cdot (18 \cdot \mu \cdot D_i)^{-1}$
$T_{0C}$	mainstream flow temperature
$U_{jet}$	impingement velocity

### GREEK

$\eta_c$	capture efficiency
$\rho$	density of flow
$\rho_d$	particle density
$\mu$	dynamic viscosity

### INTRODUCTION

A modern issue related to the operation of gas turbine engines is the ingestion of dirt and other fine particles that lead to blockages of cooling holes and passages [1]. This issue is particularly important in considering the range of cooling features required to effectively cool combustion chamber walls from the hot gases of combustion. As the need to fly in environments with high particulate concentrations rises [2], the criticality of operations in these environments also increases.

Many gas turbine engines employ a double-walled combustor liner with impingement and effusion cooling. Impingement cooling enhances the backside cooling of the hot wall while effusion cooling creates a protective film of coolant along the hot wall exposed to the hot main gas path. Dirt accumulation on the internal and external surfaces creates undesired thermal characteristics and can block cooling holes that severely diminishes the cooling capability of these designs.

This study investigated five double-walled coupon designs for reduced dirt accumulation by integrating different surface features on the effusion wall impacted by the cool impingement jets. The experiments were conducted at room temperature and used AFRL 05 dirt with particle diameters of 0-3  $\mu\text{m}$ . Two dirt injection modes were used that consisted of a slug and continuous to mimic sudden bursts and continuous feeds of dirt, respectively.

## LITERATURE REVIEW

Particulates ingested by the hot section of a gas turbine engine present several issues linked to the performance of engine components. Particles comprised of ash [3] and dust [4] deposit on turbine blades and combustor walls causing severe erosion [5]. This erosion can dramatically reduce the life-span of engine components [6]. Deposition of particulate can also plug internal cooling channels and film cooling holes thereby reducing cooling effectiveness, resulting in components that exceed their melting temperatures [7]. Numerous studies that evaluate particulate deposition mechanics have been, and continue to be, conducted to develop correlations for the design of deposition resistant geometries.

Moroianu et al. [8] showed that the air-intake of gas turbine engines ingests particles across a range of sizes while operating near the ground. The particles then enter the compressor where they may collide with and damage compressor blades [9]. This particulate-air mixture flows through secondary air circuits in which the high-pressure air is used to cool the hot section components. Schneider et al. [10] found that as particulate passes through the bypass ducts, the particulate collides with the duct walls and breaks into various smaller sized particles that can block cooling features. Furthermore, a study conducted by Whitaker [11] showed that the particulate size distributions had different effects on flow blockage. Particles smaller than 5 microns had a strong tendency to deposit onto a surface and form loosely packed structures which led to flow blockage. However, particles larger than 5 microns maintained a higher kinetic energy which broke apart the loosely packed structures on impact rather than sticking to the surface. Amongst all the size distributions tested, it was found that particles under 3.25  $\mu\text{m}$  were the primary cause of blockage.

Once in the turbine hot section, the high temperatures soften the particulate which may cause more dirt deposition and sticking to cooling geometries [12]. In addition to softening, the increased temperatures reduce the normal coefficient of restitution, which means that the particles have less kinetic energy to rebound and hence are more likely to stick [13]. Yang et al. [14] confirmed, amongst other things, that velocity and temperature were significant factors for controlling this sticking behavior between particles and surfaces. Crosby et al. [15] found that deposition began when the gas temperature exceeded 960°C. The capture efficiency was also shown to increase non-linearly with increasing temperatures in a single impingement cone [16].

Despite the challenge, computational studies have tried to simulate particle deposition within gas turbine engines with varying results. Singh et al. [17] simulated sand transport within the internal cooling passages of a turbine blade with a particle size distribution of 0.5-25  $\mu\text{m}$ . The results showed that sand particles followed experimental flow paths favorably and could be used to predict damage prone areas. Ai and Fletcher [18] modeled particulate deposition on a high-pressure turbine blade and found good agreement between computational and experimental capture efficiencies. Furthermore, it was found that capture efficiency decreased with increased blowing ratio and increased hole size (when the blowing ratio was held constant). Blunt et al. [19] studied particle deposition in turbine cooling holes using 0-10  $\mu\text{m}$  particulates. The computational model accurately predicted deposition caused by the impinging flow and also showed that deposited particles within the effusion holes were mostly 0.5-1.2  $\mu\text{m}$  in size.

Experimental studies that evaluate particle deposition in double-wall combustor liners are limited. Of these studies, Cardwell et al. [20] compared four combustor liner designs with different hole spacings at ambient temperature with pressure ratios between 1.02 and 1.1. For all liners tested, they found that the Stokes number increased as the pressure ratio increased, which led to more particle-wall collisions and cooling hole blockages. Furthermore, staggered impingement and effusion holes resulted in less blockage than overlapping holes. Land et al. [1] confirmed these findings, showing that blockage increased at pressure ratios below 1.1. However, at pressure ratios greater than 1.1, impingement velocities increased which resulted in more particle fragmentation that reduced the blockages. Additionally, Land et al. showed that the spacing between impingement and effusion plates is critical for particle fragmentation. When the spacing is small, particle breakup is adversely affected by interactions between the impingement jets and flow between effusion holes, but at large spacings, the jet strength is reduced which limits particle fragmentation. A study conducted by Cory et al. [21] evaluated dirt loading rates on a double-walled combustor liner using burst and continuous feed mechanisms. They found that bursts of dirt resulted in higher dirt capture than a slow continuous feed, indicating that the dirt loading rate is an important factor for dirt accumulation. Despite the increased dirt capture, the dirt patterns in both feed types remained unchanged. While the combustor liner modifications discussed here have been fruitful for reducing particle deposition, studies that investigate how surface topography alters particulate deposition in combustor liners have been neglected.

The purpose of the current study is to provide an evaluation of the effects that unique surface features have on particle deposition in a double-walled combustor liner. Effusion plates with different surface features extruded from the cold-side surface are assessed for reduction of particulate deposition. The study identifies several unique combustor liner cooling designs that are less sensitive to dirt deposition which leads to a reduction in turbine maintenance.

## EXPERIMENTAL FACILITY AND METHODOLOGY

A schematic of the test facility used in this study is shown in Figure 1. The facility incorporated two different dirt injection modes: slug and continuous. In the slug feed method, dirt was split into three portions of equal mass, referred to as slugs. Each slug was sequentially placed into the slug feed chamber located upstream of the coupons. The chamber was then slightly pressurized above the mainstream flow pressure and opened using a ball valve that injected the dirt into the system.

For the continuous feed method, Cory et al. [21] developed a method such that dirt was spread evenly along a zinc-coated plate located in the continuous feed chamber shown in Figure 1. To inject dirt in a continuous manner, a small capillary tube aimed at the plate was traversed externally by a stepper motor to uniformly inject air into the dirt, causing the dirt to be dispersed into the coolant flow.

As shown in Figure 1, downstream of where the dirt was injected, the flow entered a clear, rectangular plenum with a splash plate at the start to ensure uniformity. A filter box was attached to the backside of the effusion plate to prevent dirt from scattering into the laboratory environment.

A regulated flow controller with a standard accuracy of  $\pm$  (0.8% reading + 0.2% of full scale) was used to measure and control the mass flow rate during the experiments while maintaining a constant supply pressure. Pressure taps were located upstream and downstream of the coupon to quantify the pressure ratio across the coupon. Pressure transducers with an accuracy of  $\pm$  0.08% Best Straight Line (BSL) maximum were attached to the pressure taps to measure the upstream and downstream pressures. The pressure ratio is the ratio of the supply fluid pressure to the exit static pressure as shown by Figure 1 and is calculated as

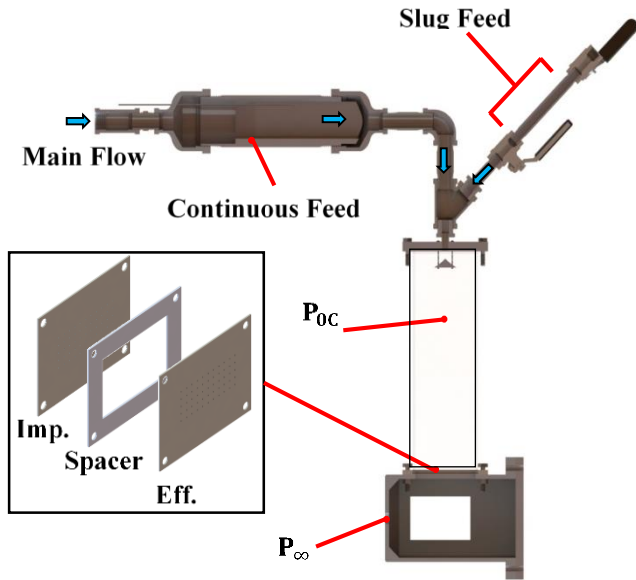


**Figure 1. Diagram of the dirt test facility emphasizing the locations of the feed types and coupons.**

$$PR = \frac{P_{0c}}{P_{\infty}} \quad (1)$$

The flow parameter defined in Equation 2 was used to scale the flowrate. As particulate flowed through the double-walled coupons, some of the effusion plate holes became blocked, which required a need to reduce the mass flow rate through the impingement plate as a means of maintaining a constant pressure ratio during testing. This decrease of the mass flow rate caused a reduction in the flow parameter (FP), which was monitored for the duration of the testing using the impingement plate as the metering section.

$$FP = \frac{4\dot{m}\sqrt{RT_{0c}}}{\pi P_{0c}ND_i^2} \quad (2)$$

Across all of the tests in this study, the only parameter that changed in the FP equation was the mass flow rate. As a result, the dirt deposition results were driven by the average jet velocity. However, FP was still used as the main flow field indicator so that comparisons can be made to experiments with different testing parameters in future studies.

Despite the impingement plate being the metering section for the FP, the desired pressure ratio was for a pressure drop across the entire coupon. Due to the small size of the scaled parts, a pressure drop could not be directly measured across the impingement plate. However, CFD simulations across the five tested designs gave an equivalent pressure ratio of 1.006 across the impingement plate, compared to the 1.045 overall desired pressure ratio. Note that this CFD did not include dirt buildup, but the clean simulation results suggest that using the overall PR is sufficient for the FP calculations.

To compare the performance of each of the double-wall designs, the capture efficiency defined in Equation 3 was calculated. The mass of the effusion plate was measured before ( $M_{cl}$ ) and after ( $M_{eff}$ ) each test to quantify the amount of dirt deposited on the effusion plate. This value was then divided by the total mass of dirt injected into the system that successfully reached or passed through the coupon ( $D_{int}$ ). As will be discussed in the next section, all dirt was tracked and accounted for to quantify  $D_{int}$ . Note that low capture efficiencies are desirable, which represents low dirt deposition.

$$\eta_c = \frac{M_{eff} - M_{cl}}{D_{int}} * 100 \quad (3)$$

The percent reduction in flow parameter (RFP) defined in Equation 4 was evaluated for each of the coupons. The RFP is based on the flow parameter measured before and after dirt was injected for a given pressure ratio.

$$RFP = \frac{|FP_{clean} - FP_{dirty}|}{FP_{clean}} \quad (4)$$

Air was supplied to the test coupon from a compressed air line at ambient temperature conditions. Tests were conducted at pressure ratios between 1.02 and 1.1 with 2 grams of dirt. Due to the shape of each coupon, the mass flow rate required to achieve a given pressure ratio fluctuated and altered the jet Reynolds number ( $Re_d$ ). It was found that  $Re_d$  ranged from 1143

to 1780 and all coupons had a Mach number (Ma) below 0.1 in the impingement jet.

## DOUBLE-WALL COOLING GEOMETRY

Multiple double-wall combustor liners with impingement, spacer, and effusion plates were used for this study. Models for the baseline, swirl, elliptical pin, pin-cone staggered, and pin-cone aligned effusion plates are shown in Figure 2. Dimensions for the test coupons are given in Table 1. For all double-wall liners, a single impingement plate containing cooling holes perpendicular to the surface was used and placed upstream of the effusion plates which had holes angled at  $30^\circ$ . The 1.6 mm thick spacer plate was located between the 1.03 mm thick impingement and effusion plates. Despite having surface structures of different heights, the  $H/D_i$  remained a constant 2.2 for all impingement and effusion plate combinations except the baseline effusion plate, which maintained an  $H/D_i$  of 1.6.

For the coupons with effusion plate surface structures, some material was removed from the surface to fit the structures within the spacer gap. In doing so, the thickness of the effusion plates with surface geometries was halved, which shifted the inlet of the effusion holes closer to the cones since they no longer extended as far. Because of this modification, the  $H/D_i$  for the effusion plates with geometries was greater than that tested for the baseline effusion plate. However, testing of the baseline effusion plate at the  $H/D_i$  ratio of 2.2 produced similar results to the full baseline effusion plate tested at an  $H/D_i$  of 1.6.

**Table 1: Coupon Test Geometries**

Impingement Plate			Effusion Plate		
$D_i$ [mm]	$S_1/D_i$ and $S_2/D_i$	$A_f$ [mm <sup>2</sup> ]	$D_e$ [mm]	$S_1/D_e$ and $S_2/D_e$	$H/D_i$
1.03	6.2	45.7	0.8	7.9	2.2

All impingement and effusion plates contained 55 holes in a  $5 \times 11$  ( $S_1 \times S_2$ ) array, which represented a portion of an actual combustor liner, and were printed using an SLA 3D printer with a higher temperature resin. A thin layer of black paint on all impingement and effusion plates ensured a smooth surface roughness across all designs.

## DIRT CHARACTERIZATION AND TRACKING

All experiments used AFRL 05 dirt which is dominantly composed of quartz and gypsum. Cory et al. [21] reported that the dirt had a nominal particle diameter which ranged from 0 to  $3 \mu\text{m}$  with a mean diameter of  $1.2 \mu\text{m}$ ; a cumulative size distribution and density of the dirt is also given by Cory et. al. [21]. Using the mean particle diameter and the velocity through the impingement jet, the Stokes number (St) of the individual dirt particulate was calculated and found to be lower than 0.3 for all tests. This calculation neglected any clumping effects that may have occurred as particulates were funneled through the impingement jets. Using the entire range of particle sizes gives a maximum Stokes number of 1.9. However, the

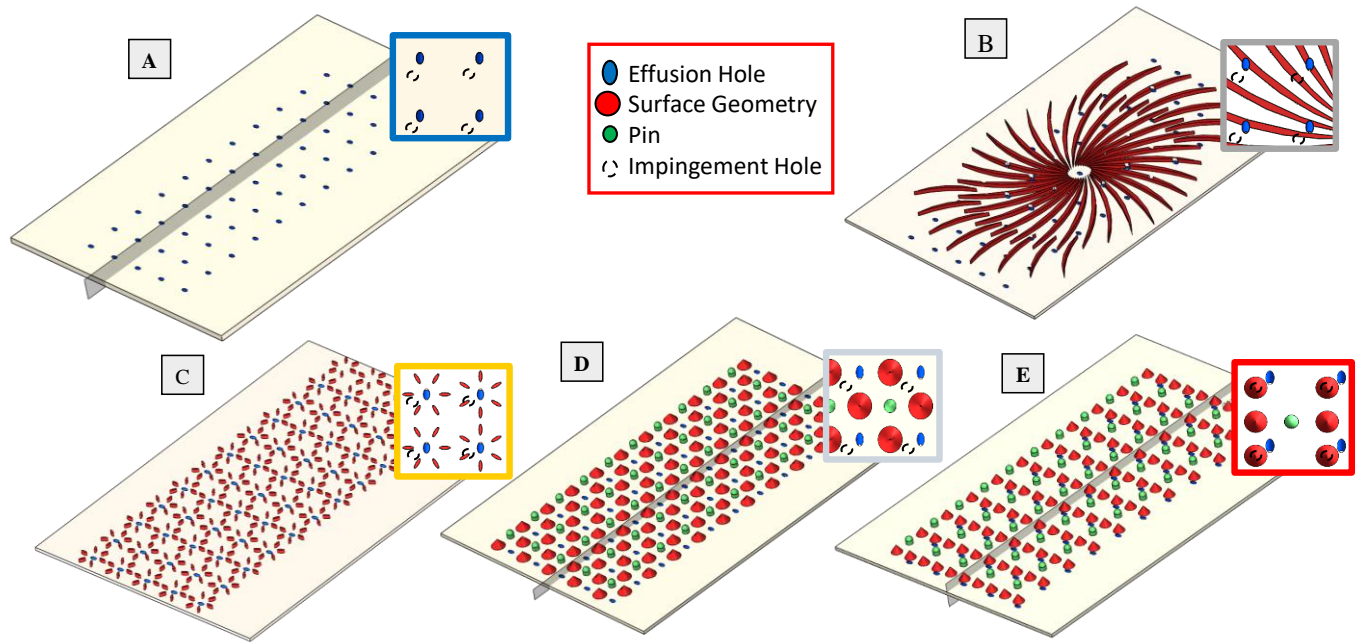


**Figure 2. SolidWorks models of all effusion plates. From left to right, (7a) baseline, (7b) swirl, (7c) elliptical pin, (7d) pin-cone staggered (PCS), (7e) pin-cone aligned (PCA). The black planes shown in 7a, 7d, and 7e reference the location of the contour plots used for computational simulations.**

cumulative particle size distribution from Cory et. al. [21] shows that most of the dirt diameters are close to the 1.2  $\mu\text{m}$  mean. As a result, using the mean particle size for the Stokes number calculation is most applicable to this study. Prior to testing, the AFRL 05 was baked for four hours to remove the humidity and sifted through using a coarse wire mesh to remove clumps.

To achieve accurate values for the capture efficiency, dirt was tracked to identify how much dirt successfully reached the coupon. The dirt often collided with and stuck to surfaces upstream of the coupon. The dirt that did not make it to the coupon was removed from the mass of dirt ( $D_{\text{int}}$ ) that entered the coupons. Figure 3 shows the percentage of dirt that was found and where it was located for each of the five coupon designs tested. Larger percentages of dirt were lost in the piping and the plenum. Through tracking, 80-90% of the dirt was located and the remainder was assumed to have passed through the coupon such that capture efficiency could be calculated.

Multiple-sample repeatability tests were performed given the repeatability was the key driver of the uncertainty. Shown in Figure 4, fifteen tests with each feed type were performed on a double-walled impingement plate and the results were grouped into five sets of three. A student-T distribution for a confidence interval of 95% was used to find the precision uncertainty. These values were reported in percent of the mean in Table 2. The results indicate that the precision uncertainty of the capture efficiency is 5.6% for slug and 8.1% for continuous flows, which required three samples for every condition to be tested. All other values reported precision uncertainties lower than 5% for slug and continuous feed configurations.

## COMPUTATIONAL SETUP

A computational fluid dynamics (CFD) simulation was conducted on a full section of the baseline, pin-cone staggered (PCS), and pin-cone aligned (PCA) geometries as described by Figure 2. Note that dirt was not included in the simulations. A

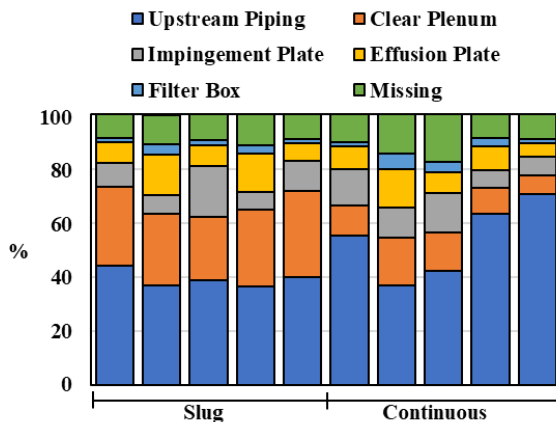


Figure 3. Percentage of dirt by location for all test cases at a PR of 1.045 with 2g of dirt.

commercial CFD code STAR-CCM+ [22] was used to investigate the relationship between the flow field and experimental dirt deposition. A steady Reynolds Averaged Navier-Stokes (RANS) simulation with a shear-stress transport (SST)  $k-\omega$  turbulence model was used. The fluid was treated as an incompressible, ideal gas. Simulations were done without particles with the goal of understanding the flow fields. The boundary conditions included a stagnation inlet and atmospheric pressure outlet, which gave a pressure ratio of 1.045. Figure 5 displays the locations where the boundary conditions were applied.

A hexahedral mesh was constructed using a prism layer mesher, surface remesher, surface wrapper, and trimmer. The mesh used for the simulation consisted of 4 prism layers, with a base cell size of 0.2 mm and a minimum mesh size of 10.1M total cells for all CFD cases. For the pin cone designs, the mesh was as large as 20 million cells due to the extra surface area of the pins and cones. Figure 5 shows the mesh region near the slanted effusion holes. Grid independence was evaluated by varying the cell size from 4.85M to 10.1M. In this range, the jet Reynolds number varied by a maximum of 1.2%. The average  $y^+$  values on all surfaces was 0.2 and the maximum was 3, so the solver did not use wall functions and resolved the near wall boundary layers. All simulations reached normalized residual levels below  $1e-4$  and were not changing after 1000 iterations, although initial simulations were run to 2000 iterations to

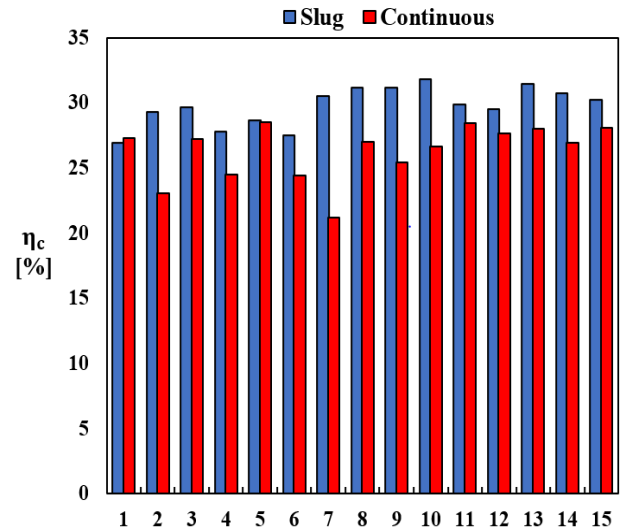


Figure 4. Capture efficiency results for precision uncertainty analysis at a PR of 1.045 with 2g of dirt.

Table 2: Precision Uncertainty Results

PR	1.045	
Test Type	Slug [%]	Continuous [%]
Capture Efficiency	5.6	8.1
Flow Parameter	2.5	3.3
% of Dirt Located	2.3	3.9



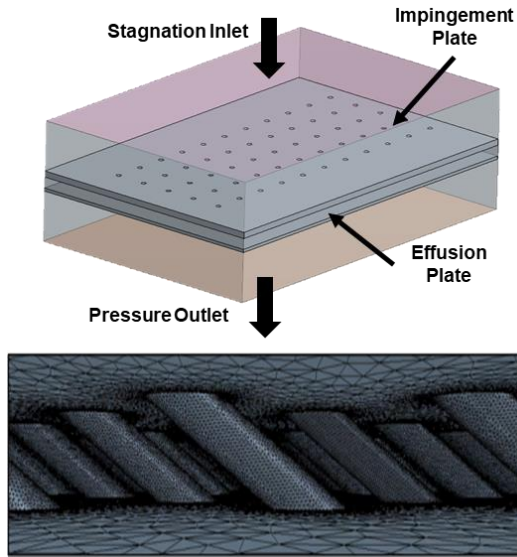


Figure 5. The top image shows the computational domain and boundary conditions. The bottom image shows the mesh region in and around the effusion holes.

confirm. The mass flow rate imbalance between the inlet and the outlet of the CFD domain was less than 0.1% after 1000 iterations.

### DIRT DEPOSITION PATTERNS

Dirt deposits on the cold-side (inner wall) of the effusion plates, which were tested at a PR of 1.045 with 2 g of dirt, are shown in Figures 6a-e. The colored outlines of each image matched to those shown in Figures 2a-e as well as the legend in Figures 2a-e. In Figures 6a-e, the entrance to the effusion holes is shown with minimal dirt while the peak mounds of the dirt are aligned with the impingement jet location that exits on the opposite wall. The baseline effusion plate in Figure 6a showed the most prominent dirt deposits relative to all other geometries evaluated. The dirt pattern in Figure 6a shows uniform dirt “peaks” that taper off in the radial direction. Between the dirt peaks are also straight lines of dirt, referred to as “ridges”. These ridges are located mid-way in all directions between the impingement dirt peaks. As the adjacent jets radially spread, a stagnation location occurs where dirt drops out of the coolant to form a ridge of dirt.

The swirl plate in Figure 6b prevented the formation of the dirt ridges found between impingement jets relative to the

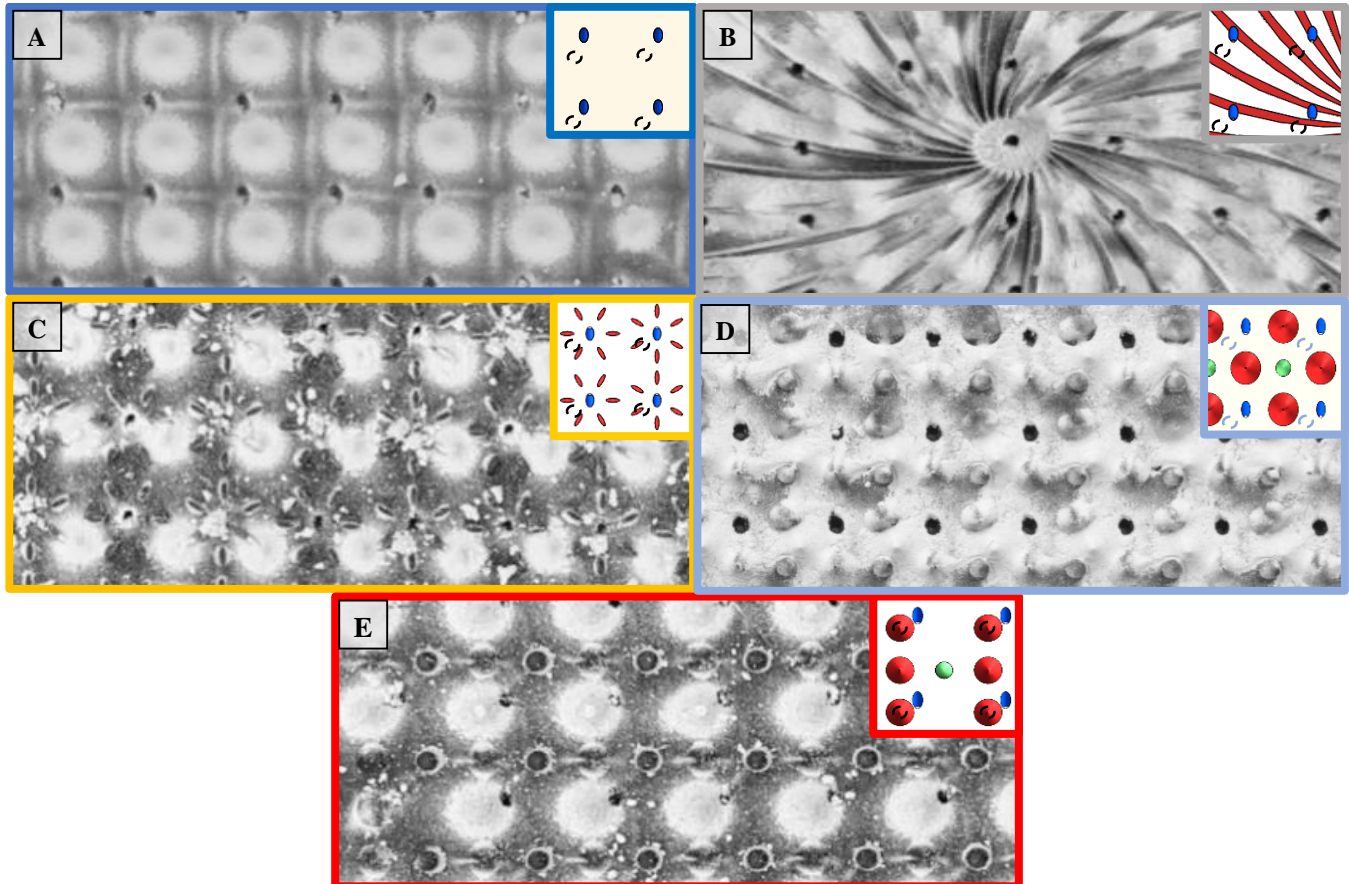


Figure 6. Post-slug feed test results of effusion plates paired with a 1 mm jet diameter impingement plate at a PR of 1.045 with 2 g of dirt. From left to right, (6a) baseline, (6b) swirl, (6c) elliptical pin, (6d) pin-cone staggered (PCS), (6e) pin-cone aligned (PCA).

baseline. Ridges were unable to form due to the curved channels that were extruded from the effusion plate's surface which prevented the radially spreading impingement jets from colliding with each other. However, large diameter dirt peaks persisted where the impingement jet impacted the effusion plate's surface. These peak regions indicate that the impingement was a dominating flow feature despite any type of channeling effect from the plate design.

On the elliptical pin plate in Figure 6c, both the diameter and height of the dirt peaks were reduced relative to the baseline. Unlike the baseline in Figure 6a, no secondary dirt ridges were formed because the elliptical pin fins disrupted the stagnation location of the merging impingement jets. Instead, dirt deposited around the elliptical pins which is indicated by the white outline surrounding each pin. Despite having eliminated the dirt ridges and reduced size of the dirt peaks, more dirt deposited and blocked the effusion holes. This increased blockage is likely caused by a channeling effect created by the elliptical pins surrounding the effusion hole which aided in reducing the size of the dirt peaks.

The pin-cone staggered (PCS) effusion plate in Figure 6d showed a nearly uniform spread of dirt across the surface relative to the other double-wall configurations. As the flow impinged on the surface, it deposited dirt between the pins and cones rather than funneling the dirt directly through the effusion holes. This behavior indicated that the placement of the pins and cones on the PCS geometry was effective at modifying the flow near the wall, though this particular staggered pin-cone configuration produced undesired dirt deposits.

By changing the placement of the pins and cones, the pin-cone aligned (PCA) effusion plate shown in Figure 6e eliminated dirt ridges, reduced the diameter and height of the dirt peaks, and prevented the spread of dirt as seen in Figure 6d for the PCS. Note that the cones are aligned with the impingement jets for the PCA case. The thin ring of deposition around the pins on the PCA plate, which are located in the four corners surrounding the impingement site, indicate that the pins are interrupting the radial spread of the jet after impingement. Due to the close proximity of the cone and effusion hole on the PCA plate, the dirt appears to more readily pass through the effusion hole after impinging on the cone which may further explain why dirt did not spread across the surface like the PCS plate shown in Figure 6d.

The correlation between the experimental dirt deposition patterns in Figures 6a with that predicted by CFD are shown in Figure 7. The CFD prediction for the baseline geometry shown in Figure 7a highlights the near-wall velocity magnitude located 0.04 mm above the cold effusion plate wall. The impact location of the impingement jet is denoted by a dashed black line and the effusion hole is denoted by a dashed red line. Comparisons of the CFD predicted near-wall velocities and the experimental dirt deposition shows a correlation between stagnant regions and observed dirt deposition. The locations on the plate with lower predicted velocities relative to their surroundings in the CFD study often had correlations to areas of heightened dirt deposition in experiments as seen by the

white dirt in the Figure 7b. This phenomenon is especially evident with the stagnation region at the impact location of the impingement jet on the effusion plate where a conical dirt mound was experimentally observed. The CFD predicts that a higher normalized velocity region surrounds the center stagnation region, which decreases in velocity magnitude as the radial distance from the impact region increases. In this region between the impact and ridges, the dirt flowed with the velocity flow field, which resulted in little to no dirt deposition until the stagnant ridge region. The areas that lacked dirt deposition are denoted by the dark regions between the dirt peak and ridges of the experimental results in Figure 7b. This dirt observation suggests that the small, low Stokes number dirt particles follow the velocity flow field until they cannot anymore.

In Figure 7c, CFD predictions of the velocity gradients based on Equation 5 were plotted in a plane within 35  $\mu\text{m}$  of the baseline effusion plate surface. These CFD results are provided in a grayscale contour, which allows for interesting comparisons to the observed dirt depositions which are similarly colored.

$$\left| \frac{du}{dx} + \frac{dv}{dy} \right| * \frac{U_{\text{jet}}}{D_i} \quad (5)$$

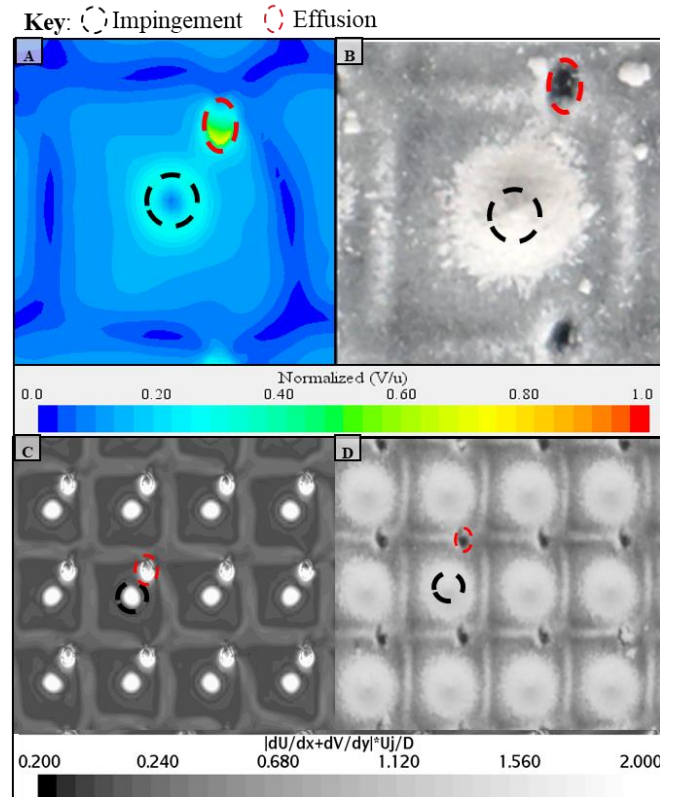


**Figure 7. Computationally predicted near-wall velocity profile (7a) and near-wall velocity gradients (7c) compared to experimental dirt deposition test results (7b and 7d) of the baseline effusion plate (black is impingement; red is effusion).**

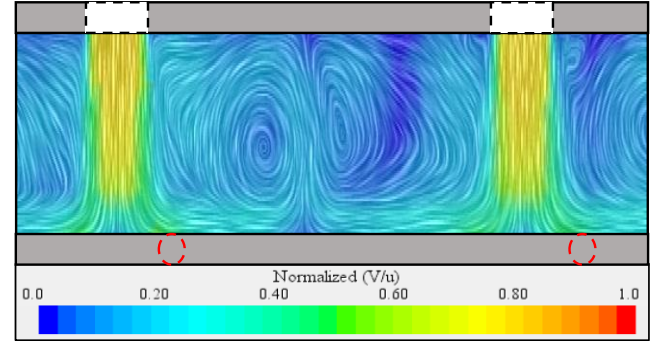


Overall, the velocity gradients show that the areas with high velocity gradients correlated to the areas of heavily observed dirt deposition, namely at the location of impingement jet impact and the ridge regions. Similarly, the areas with small velocity gradients resulted in little to no dirt deposition. This comparison supports the suggestion that the low Stokes number dirt particles follow the flow field until they cannot anymore, which makes the plotting of the parameters of Equation 5 a reasonable estimate of the deposition patterns.

Figure 8 shows the flow field between the impingement and effusion plate for the baseline geometry from a side view. The location where the flow field was evaluated is denoted by the black plane shown in Figure 2a. The flow field clearly shows the vortex pattern that correlates well with the ridges of dirt deposition that was shown in Figure 7. This vortex region agrees with the high velocity gradients shown in the ridge region in the CFD of Figure 7c. As the adjacent impingement jets impact the backside of the effusion plate, there is an intersection between vortices that develop outside of the impingement area. This intersection results in a stagnation region in which the dirt deposits onto the plate. The stagnation region at the impingement jet impact is also seen in Figure 8, which again correlates well with the dirt deposition in this center region.

Also, shown in Figures 9a-h, the computational and experimental results of the PCA (aligned) plate were compared to that of the PCS (staggered) plate by taking similar contours from those in Figure 7. As shown in Figure 9a and b, the CFD flow field for the PCA plate predicted stagnation/low velocity

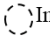

Key:  Impingement  Effusion



**Figure 8.** Computationally predicted side velocity flow field showing vortices between the impingement and effusion plate which enabled the dirt ridges to form in the baseline plate. The in-plane impingement holes are denoted by dashed black lines and out-of-plane effusion holes are denoted by dashed red lines.

regions at the base of the cones and at a small radial distance from the cones; dirt was experimentally deposited at these locations with a radius similar to the onset of the low velocity region predicted by the CFD. This contour suggests that the small dirt particles follow the near wall velocity flow field until a stagnation region is encountered.

Additionally, Figure 9c and 9d suggest that high velocity gradients occur at the base of the cone and in the ridge regions

Key:  Impingement  Effusion

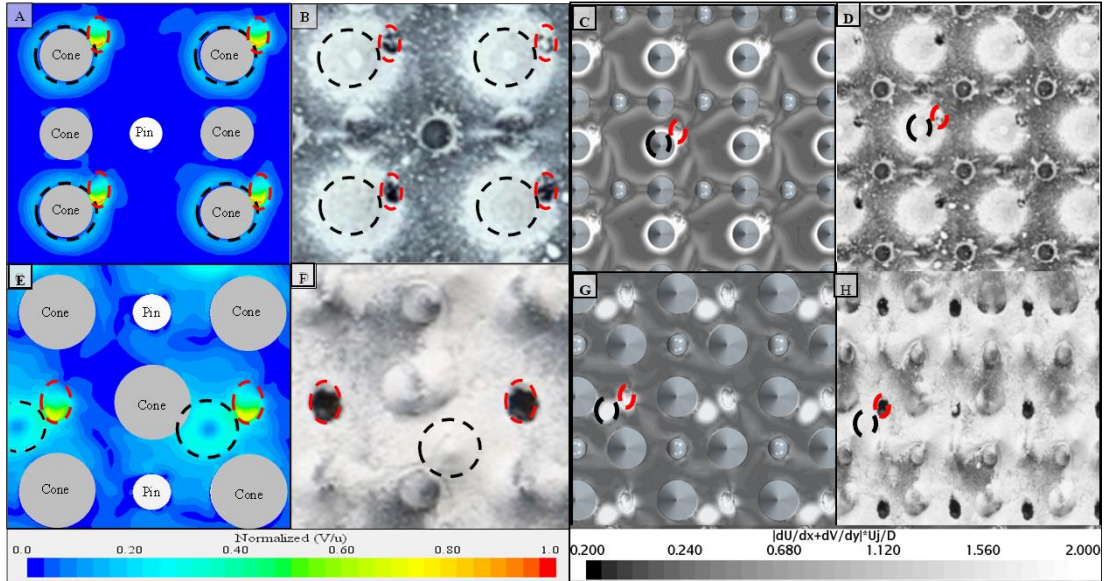


**Figure 9.** Computationally predicted near-wall velocity profile (9a and 9e) compared to the physical dirt deposition test results (9b and 9f). Computationally predicted near-wall velocity gradients (9c and 9g) compared to the physical dirt deposition test results (9d and 9h) of pin-cone aligned (PCA) plate (top) and pin-cone staggered (PCS) plate (bottom). The impingement jet on the effusion plate is denoted by a dashed black line and the effusion hole is denoted by a dashed red line.



between the pins and cones, which were the areas of heightened dirt deposition. Unlike the baseline effusion design where ridges formed in all radial directions from the impingement jet, the only ridge regions for the PCA design were between the cones and pins. Comparisons of the velocity gradient plots for the PCA in Figure 9c to the velocity gradient plots for the baseline effusion plate in Figure 7 show that the ridge regions with high velocity gradients correlated with the observed ridge formations for each the respective designs.

The PCS plate predicted higher velocities, more stagnation regions, and more high velocity gradients across the surface of the coupon relative to the PCA. The experimental results for the PCS show increased levels of dirt occurred across the surface where the high velocity regions and high velocity gradient regions existed in the CFD. These findings indicate the importance of the near-wall velocities. By placing the cone directly in the path of the impingement jet, the flow path in PCA was modified such that dirt deposited near the cone rather than spreading across the plate.

Figure 10 compares the flow field between the effusion and impingement plates for the PCS and PCA geometries. The location of the plot is shown by the black planes in Figure 2d-e. The velocity profile of the PCS geometry in Figure 10 showed a distinguished stagnation region at the area of direct impingement. By aligning the cone with the impingement jet in the PCA case, the flow around the conical structure prevented direct impingement on the effusion plate surface, resulting in reduced dirt deposition. Instead of having a stagnation region directly beneath the impingement jet, the CFD predicted formation of a stagnation region at the base of the cone. As dirt accumulation begins at the base of the cone, the stagnation

region is believed to move up the cone and hence explains the deposition of dirt up the surface of the cone. In both configurations shown in Figure 10, a near-wall vortex formed in the gap between the conical structures which was caused by the out of plane effusion holes and the intersecting of the radially spreading jets. Since the conical structures were not aligned with the impingement jet on the PCS plate, a second vortex formed midway up the spacer. The formation of a secondary vortex in the PCS geometry further contributed to the increased deposition. Note that both the magnitude and vortex pattern formed in the PCA plate were dramatically different compared to the PCS plate. By having smaller vortices introduced near the wall, the PCA plate resulted in lower dirt accumulation.

### CAPTURE EFFICIENCY RESULTS

As was discussed, the figure of merit for comparing the various geometries was the capture efficiency, which quantifies the amount of dirt that remained on the effusion plate relative to the amount delivered to the double-wall coupon. The capture efficiency of each coupon is shown in Figure 11 in which slug feed tests are denoted by solid bars and continuous feed tests with dashed bars. In general, continuous feed tests resulted in lower capture efficiencies than slug feed tests, but gave the same relative trends between geometries.

The capture efficiency of the baseline coupon reached 42% for both slug and continuous feed tests. Note that the capture efficiency for the baseline coupon at an  $H/D_i$  of 2.2 was 38%, which was within the precision uncertainties reported earlier in Table 2 for the baseline effusion plate at  $H/D_i$  of 1.6. The swirl

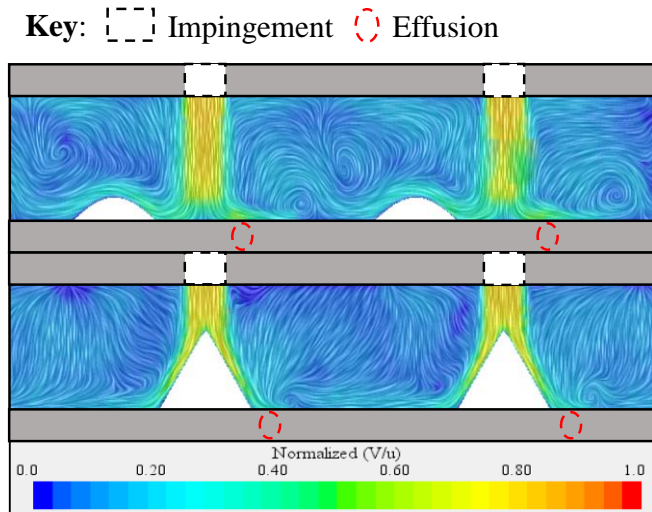


**Figure 10.** Computationally predicted side velocity profile of the pin-cone staggered (PCS) plate (top) and pin-cone aligned (PCA) plate (bottom). The in-plane impingement holes are denoted by dashed black lines and out-of-plane effusion holes are denoted by dashed red lines.

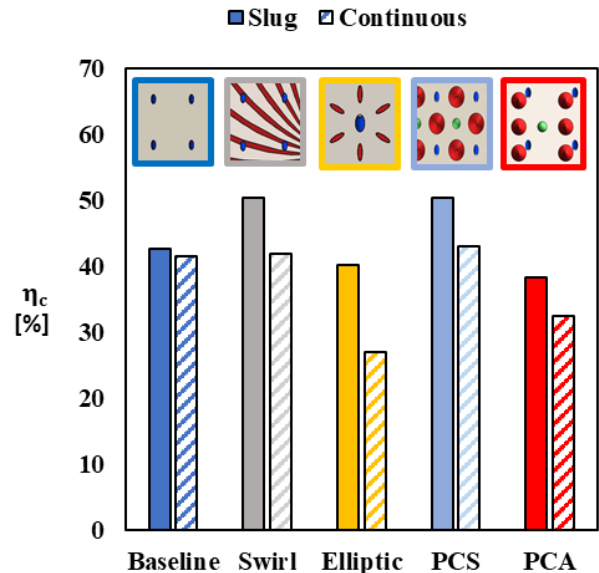


**Figure 11.** Capture efficiencies for impingement and effusion coupon pairs at a PR of 1.045 with 2g of dirt.

and PCS plates performed the worst, with capture efficiencies near 50% for slug feed and at or above baseline for continuous feed tests. For both cases of the swirl and PCS, the dirt was spread across the surface rather than concentrated only into peaks explaining why the capture efficiencies were higher as shown in Figure 11.

The elliptical pin and PCA geometries performed better than the baseline geometry, with capture efficiencies below baseline for both slug and continuous feed tests. For both the elliptical pin and PCA cases, dirt concentrated into peaks and did not spread across the surface as the swirl and PCS geometries did. This reduction in capture efficiency is a result of the shape and placement of the pins and cones which caused a change in the near-wall velocity. For the elliptical pin and PCA geometry, this change in the flow field created a funneling effect through the effusion hole and reduced the spread of dirt deposition.

### SCALING CAPTURE EFFICIENCY

To evaluate the scaling of capture efficiency as a specific function, the dirty plate flow parameter ( $FP_{dirty}$ ) was determined for all geometries as shown in Figure 12. Note that each coupon had a different flow parameter despite operating at a constant pressure ratio. The flow parameter before dirt injection ( $FP_{clean}$ ) was also examined, but the data produced a similar trend to that in Figure 12. Slug feed tests are represented by filled markers and continuous feed tests by open markers in Figure 12. The data in Figure 12 shows a clear trend of increased capture efficiency with increased flow parameter. Figure 12 indicates that the best performing coupons in terms of capture efficiency,

namely PCA for slug feed tests and elliptic pin for continuous feed tests, had the lowest flow parameters.

As  $FP$  increased, the mass flow rate also increased leading to higher jet impingement velocities which caused dirt to deposit on the surfaces. The jet Reynolds number of the impingement plate was also examined, but the data produced a trend identical to Figure 12 and therefore did not provide better scaling than the  $FP$ .

Shown in Figure 13 are the reduction in flow parameter (RFP) values for each of the tested geometries. The flow parameter reductions throughout testing are caused by the small dirt particles clogging the effusion cooling holes. As such, smaller RFP's suggest that less blockage occurs. From the results of Figure 13, the swirl, PCS, and PCA effusion designs had less  $FP$  reductions than the baseline case, with the PCS and PCA designs being the best with the lowest cooling hole blockage from the dirt particles.

It is interesting that the PCS had a lower reduction in  $FP$  than the PCA design because the PCS geometry had a higher capture efficiency than the PCA design. This result indicates that despite having more dirt deposition, and hence potential of cooling hole blockage, the PCS did not impact the flow as much as the PCA design. A possible explanation for this result could be that the flow fields imparted by the PCS designs focused more of the dirt deposition onto the effusion plate surface as opposed to through the cooling holes. CFD predictions in Figure 9 show more velocity contours spread out across the PCS coupon compared to those shown for the PCA geometry, which shows velocity contours that funnel the flow into the effusion holes. As a result, for the PCS coupon, less dirt was pushed through the coupon cooling holes and hence less blockage occurred, but this was done at the expense of having a higher capture

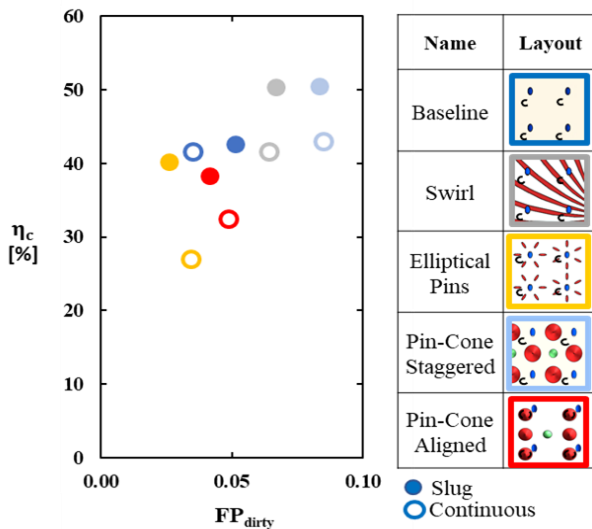


Figure 12. Capture efficiency as a function of average flow parameter at a PR of 1.045 with 2g of dirt.

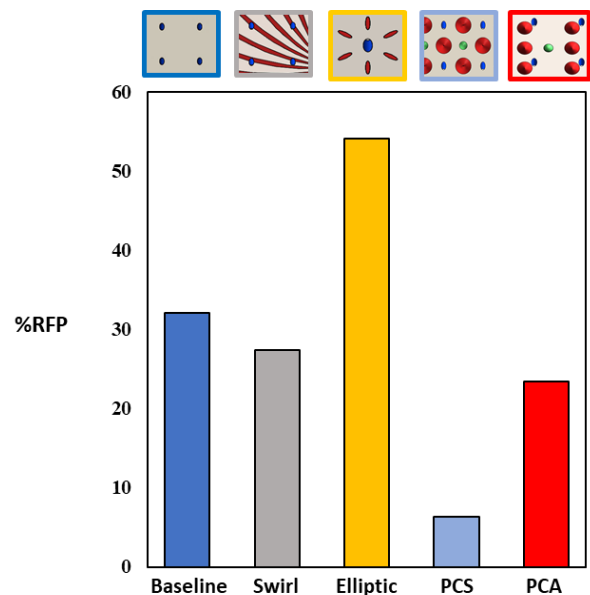


Figure 13. RFP for each of the tested coupons at a PR of 1.045 with 2g of dirt.

efficiency. In contrast, the PCA structure could have the reverse effects where more flow was funneled towards the effusion cooling holes, and as a result, less dirt settled on the effusion plate surface but at the expense of more flow blockage.

Despite the PCS having the lowest %RFF, the PCA geometry was determined to be the best tested design for dirt resistance because it was the only design that showed both lower capture efficiencies and lower RFP's compared to the baseline design.

Shown in Figure 14, the best overall performing double-walled liner coupon in terms of flow parameter, namely the PCS plate, was tested at varying pressure ratios (PR) and the corresponding percent reduction in flow parameter (RFP) was determined. As dirt is deposited on the coupon, the FP decreased before it reached a nearly constant level. This trend in RFP indicates that at higher PRs, the dirt deposition remains the same in terms of hole blockage.

## CONCLUSION

Experimental and computational studies on double-walled combustor liner coupons assessed how dirt deposition can be decreased when the surface of the effusion plate was modified. The experimental coupons were additively manufactured to incorporate different shapes extruded from the cold-side surface of the effusion plate. The capture efficiency and flow parameter were calculated from experimental measurements to compare the performance of each design. CFD predictions were made on several geometries to inspect the flow field and identify parameters that contribute to dirt deposition.

In this study, baseline, swirl, elliptical pin, pin-cone staggered, and pin-cone aligned effusion plates were paired with a single impingement plate and were compared in terms of dirt deposition. Of the coupons tested, only the elliptical pin and pin-cone aligned plates reduced the capture efficiency below a baseline design with only impingement and effusion holes. The dirt patterns indicated that the placement and design of the surface features for the worst performing coupons, namely swirl

and pin-cone staggered, enhanced the spread of dirt across their surfaces which resulted in higher capture efficiencies. In contrast, the elliptical pin and pin-cone dispersed the impingement jet and aided in funneling the dirt through the effusion holes. When compared to the baseline, the pin-cone aligned coupon had the best performance with a reduction in capture efficiency of 4% and 9% for slug and continuous feed respectively.

CFD was implemented to study how near-wall flow velocities can be used to predict experimental particle deposition around geometry features such as cones, pins, and holes. Studies focused on the pin-cone staggered and pin-cone aligned plates which had similar surface features but significant differences in deposition behavior. In each case, high velocity and high velocity gradient regions predicted by CFD had a correlation to locations of increased dirt concentration seen in experimental tests. The pin-cone aligned had the highest velocities surrounding the cone where the impingement jet impacted the surface. In the case of the pin-cone staggered, in which the cone was not aligned with the impingement jet, high velocity regions were seen throughout the flat surface, which correlated to measurable dirt thickness in the experiments. These computational studies show that impingement velocity modifies deposition and that higher near-wall velocities and velocity gradients result in more deposition.

To scale these findings, capture efficiency was plotted as a function of flow parameter. For flow parameters less than 0.1, the results showed that increasing the flow parameter scaled directly with increased dirt deposition. This finding exhibited that dirt deposition was a strong function of flow parameter, indicating that a low flow parameter is desired to reduce dirt deposition. A reduction in flow parameter was also measured during testing to quantify the effects of dirt blockage of the cooling holes. The pin-cone staggered and pin-cone aligned structures had the lowest RFP, indicating that these two designs had the least amount of cooling hole blockage.

The pin-cone staggered effusion plate was also evaluated at multiple pressure ratios to determine the variability in the percent reduction in flow parameter. The findings showed that the percentage reduction in flow parameter initially decreased with increasing pressure ratio before reaching a near constant level. This result showed that a double-walled combustor liner utilizing a pin-cone staggered effusion plate can run at higher pressure ratios without experiencing increased blockages in the effusion holes.

The results of this study contribute to the knowledge of dirt deposition in double-walled combustor liners and highlight several features which can be used to mitigate dirt deposition. Overall, the study showed that angled and conical structures placed on the effusion plate surface and geometrically aligned with the impingement jets were most effective at reducing dirt deposition compared to a flat effusion plate with no extruded

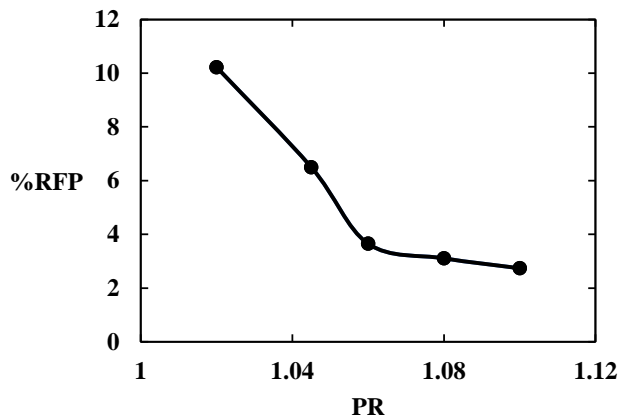


**Figure 14. Flow parameter as a function of pressure ratio for the pin-cone staggered (PCS) coupon with 2 g of dirt.**

surface features. Furthermore, the flow parameter was found to scale well with dirt deposition, which suggested that a coupon with a small flow parameter will produce less dirt deposition. While further studies are required to evaluate the dependence of deposition on cone angle, engine designers can implement the findings of this study to optimize future combustor liners.

## ACKNOWLEDGEMENTS

The authors would like to thank Pratt & Whitney and the Federal Aviation Administration for their technical and financial support of the research for this paper.

## REFERENCES

- [1] Land, C. C., Joe, C., and Thole, K. A., 2010, "Considerations of a Double-Wall Cooling Design to Reduce Sand Blockage," *ASME J. Turbomach.*, **132**(3), p. 031011.
- [2] van Donkelaar, A., Martin, R. V., Brauer, M., Kahn, R., Levy, R., Verduzco, C., and Villeneuve, P. J., 2010, "Global Estimates of Ambient Fine Particulate Matter Concentrations from Satellite-Based Aerosol Optical Depth: Development and Application," *Environ. Health Perspect.*, **118**(6), pp. 847–855.
- [3] Dunn, M. G., 2012, "Operation of Gas Turbine Engines in an Environment Contaminated With Volcanic Ash," *ASME J. Turbomach.*, **134**(5), p. 051001.
- [4] Dunn, M. G., Padova, C., and Adams, M., 1987, *Operation of Gas Turbine Engines in Dust-Laden Environments*.
- [5] Hamed, A., Tabakoff, W., and Wenglarz, R., 2006, "Erosion and Deposition in Turbomachinery," *J. Propuls. Power*, **22**(2).
- [6] Grant, G., and Tabakoff, W., 1975, "Erosion Prediction in Turbomachinery Resulting from Environmental Solid Particles," *J. Aircr.*, **12**(5), pp. 471–478.
- [7] Kim, J., Dunn, M. G., Baran, A. J., Wade, D. P., and Tremba, E. L., 1993, "Deposition of Volcanic Materials in the Hot Sections of Two Gas Turbine Engines," *ASME J. Eng. Gas Turbines Power*, **115**(3), p. 641.
- [8] Moroianu, D., Karllon, A., and Fuchs, L., 2004, "LES of the Flow and Particle Ingestion Into an Air Intake of a Jet Engine Running on the Ground," GT2004-53762.
- [9] Tabakoff, W., 1984, "Review—Turbomachinery Performance Deterioration Exposed to Solid Particulates Environment," *ASME J. Fluids Eng.* **106**(2), pp. 125–134.
- [10] Schneider, O., Benra, F., Dohmen, H.J., & Jarzombek, K., 2005, "A Contribution to the Abrasive Effect of Particles in a Gas Turbine Pre-Swirl Cooling Air System," GT2005-68188.
- [11] Whitaker, S. M., Peterson, B., Miller, A. F., and Bons, J. P., 2016, "The Effect of Particle Loading, Size, and Temperature on Deposition in a Vane Leading Edge Impingement Cooling Geometry," GT2016-57413.
- [12] Hsu, K., Barker, B., Varney, B., Boulanger, A., Nguyen, V., & Ng, W.F., 2018, "Review of Heated Sand Particle Deposition Models," GT2018-75723.
- [13] Lundgreen, R.K., 2017, "Pressure and Temperature Effects on Particle Deposition in an Impinging Flow," GT2017-64649.
- [14] X. Yang, D. Ingham, L. Ma, M. Troiano, and M. Pourkashanian, 2019, "Prediction of Particle Sticking Efficiency for Fly Ash Deposition at High Temperatures," *Proceedings of the Combustion Institute*, **37**(3), pp. 2995–3003.
- [15] Crosby, J. M., Lewis, S., Bons, J. P., Ai, W., and Fletcher, T. H., 2008, "Effects of Temperature and Particle Size on Deposition in Land Based Turbines," *ASME J. Eng. Gas Turbines Power*, **130**(5), pp. 051503.
- [16] Bowen, C. P., Libertowski, N. D., Mortazavi, M., and Bons, J. P., 2019, "Modeling Deposition in Turbine Cooling Passages with Temperature-Dependent Adhesion and Mesh Morphing," *ASME J. Eng. Gas Turbines Power*, **141**(7): p. 071010.
- [17] Singh, S., Tafti, D., Reagle, C., Delimont, J., Ng, W., & Ekkad, S., 2014, "Sand transport in a Two Pass Internal Cooling Duct with Rib Turbulators," *Int. J. of Heat and Fluid Flow*, **46**, pp. 158-167.
- [18] Ai, W., and Fletcher, T. H., 2011, "Computational Analysis of Conjugate Heat Transfer and Particulate Deposition on a High-Pressure Turbine Vane," *ASME J. Turbomach.*, **134**(4), p. 041020.
- [19] Blunt, R., S. M. Whitaker, and J. P. Bons, 2016, "The Effects of Turning Angle on Particle Deposition in Turbine Cooling Holes," AIAA 2016-4106.
- [20] Cardwell, N. D., Thole, K. A., and Burd, S. W., 2010, "Investigation of Sand Blocking Within Impingement and Film-Cooling Holes," *ASME J. Turbomach.*, **132**(2), p. 021020.
- [21] Cory, T.M., Thole, K.A., Kirsch, K.L., Lundgreen, R., Prenter, R., & Kramer, S., 2019, "Impact of Dust Feed on Capture Efficiency and Deposition Patterns in a Double-Walled Liner," GT2019-90981.
- [22] Siemens Digital Industries Software, "Simcenter Star-CCM+." 2021.